American Journal of Engineering Research (AJER)
e-ISSN: 2320-0847 p-ISSN : 2320-0936
Volume-13, Issue-7, pp-152-170
www.ajer.org
Research Paper Open Access

Computational Fluid Dynamics, Modal and Fatigue Studies of a Zero CO2 and Zero Heat Pollution Compressed Air Engine for the Urban Transport Sector

[1-] Ngang Tangie Fru; *Department of Mechanical Engineering, National Advanced School of Engineering (ENSP) University of Yaounde 1, Cameroon; ngang313@yahoo.com*
[2-] Nébo K. Yohan Arnold; *Department of Mechanical Engineering, National Advanced School of Engineering (ENSP) University of Douala, Cameroon.*
[3-] Biyémé Florent; *Department of Mechanical Engineering, National Advanced School of Engineering (ENSP) University of Yaounde 1, Cameroon.*
[4-] Kom K Yvan Armel; *Department of Mechanical Engineering, National Advanced School of Engineering (ENSP) University of Yaounde 1, Cameroon*
[5-] Kanmogne Abraham; *Department of Mechanical Engineering, National Advanced School of Engineering (ENSP) University of Yaounde 1, Cameroon.*
[6-] Ngoumkoua Wamba Chamberlin; *Department of Mechanical Engineering, National Advanced School of Engineering (ENSP) University of Yaounde 1, Cameroon.*

Resume: *The depletion of the ozone layer calls for the use of more sustainable mechanical engineering design techniques. This article highlights the use of numerical simulation approaches for computational fluid dynamics, modal and fatigue studies to further develop a kinematics and dynamics acceptable model of a zero CO_2 and zero heat pollution compressed air engine to a more efficient and structurally acceptable design. In this article we see the use of Computational Fluid Dynamics simulations to ensure a more efficient flow of fluids (compressed air) through the various conduits of the engine. You will also find the use of modal and fatigue simulations on ANSYS R18.2/2021 R2 that led to the modification of the engine structurally so that it has a longer lifespan and resist all periodic solicitations that could lead to its exponential deterioration. These studies resulted to the final design features, dimensions and material allocations of the zero CO_2 and zero heat pollution compressed air engine for the urban transport sector.*

Keywords: *compressed air engine, kinematics, dynamics, model, isothermal expansion*

Date of Submission: 16-07-2024 Date of acceptance: 31-07-2024

I. Introduction

When the natural balance of ozone destruction and production is altered more towards destruction, the term "ozone depletion" is christened (Angell & Korshover, 2005). The gases that cause a rapid depletion of the ozone layer equally fall under the greenhouse gases category (Sivasakthivel & K.K. Siva, 2011). Greenhouse gases are the main contributors of global warming (Society, 2023). These gases consisting of mainly carbon oxides, methane and CFCs, accumulated in the troposphere (8 to 16 km in the atmosphere) (Fergusson, 2001). This research work introduces us to a new area of study in the fight against heat and air pollution as it contributes to establishing a mathematical model for a zero CO_2, Zero Heat Pollution Compressed Air Engine for the urban transport sector.

A compressed air engine consists of a motor that is powered and lubricated solely on compressed air (K., et al., 2012). Compressed Air Engine technology has proven its feasibility over centuries as its designs have moved from pneumatic engines, pneumatic heated engines to compressed air engines (Malay, et al., 2021). Dennis Papin first spoke of such an engine in 1687, but it was not until 1872, that the Mekarski invented an air engine that functioned as Papin had earlier mentioned (Verma, 2008). In 1892, another heating method was introduced by Robert Hardie to improve on the range of the engine (K., P.Rathod, & Arvind S., 2012). In 1898, Hoadley and Knight, made the first urban locomotive based on the principle that the longer the air is kept in the engine the more heat it absorbed and the greater will be its range. As a result, they introduced a two-stage engine (Thipse, Compressed Air Car, 2008). Engineair Pty Ltd of Australia and Moteur Development International of France are some of the few companies nowadays that hold the international patents for the compressed air engines designs (Verma, 2008).

The zero CO_2 and zero heat pollution compressed air engine principally adapted for the cities in the Tropics will be a significant step towards generating contextualized solutions to this climate change calamity (Tian, et al., 2023). This article highlights the research done to assure the smooth flow of compressed air through the various conduits of the engine design, check the rigidity of the design to the various vibrations the engine is subjected to throughout its functioning and guarantee the design's resistance to fatigue for at least the stipulated average design lives of the materials it will be made out of.

II. Method and Material

This work is based on three major aspects of numerical studies realized on ANSYS R18.2/2021 R2; computational fluid dynamics, modal analysis and fatigue analysis. For better understanding of the principles used by ANSYS to realize these studies, we will revisit some of the underlying algebra and numerical analyses principles that govern these various studies in every ANSYS software.

2.1. Computational fluid dynamics

Applying the fundamental laws of mechanics to a fluid gives the governing equations for a fluid (Stoevesandt, et al., 2017). The conservation of mass equation is;

$$\frac{\partial \rho}{\partial t} + \nabla.\left(\rho \vec{V}\right) = 0$$

and the conservation of momentum equation is

$$\rho \frac{\partial \vec{V}}{\partial t} + \rho\left(\vec{V}.\nabla\right)\vec{V} = -\nabla p + \rho \vec{g} + \nabla.\tau_{ij}$$

These equations along with the conservation of energy equation form a set of coupled, nonlinear partial differential equations. It is not possible to solve these equations analytically for most engineering problems. However, it is possible to obtain approximate computer-based solutions to the governing equations for a variety of engineering problems. This is the subject matter of Computational Fluid Dynamics (CFD).

CFD is widely used in industry since it is more cost-effective than physical testing. However, one must note that complex flow simulations are challenging and error-prone and it takes a lot of engineering expertise to obtain validated solutions (Leer & Powell, 2021).

2.1.1. Principles of CFD

Broadly, the principles of CFD are to replace the continuous problem domain with a discrete domain using a grid. In the continuous domain, each flow variable is defined at every point in the domain. For instance, the pressure p in the continuous domain D_1 shown in the figure below would be given as

$$p = p(x), \qquad 0 < x < 1$$

In the discrete domain, each flow variable is defined only at the grid points. So, in the discrete domain shown below, the pressure would be defined only at the N grid points.

$$p_i = p(x_i), \qquad i = 1, 2, \ldots, N$$

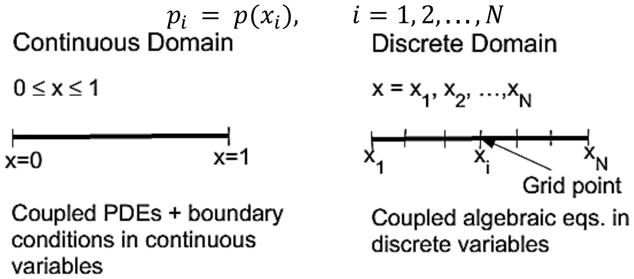

In a CFD solution, one would directly solve for the relevant flow variables only at the grid points. The values at other locations are determined by interpolating the values at the grid points. The governing partial differential equations and boundary conditions are defined in terms of the continuous variables p, $\vec{V}$etc. One can approximate these in the discrete domain in terms of the discrete variables $p_i, \vec{V_i}$ etc. The discrete system is a large set of coupled, algebraic equations in the discrete variables. Setting up the discrete system and solving it (which is a matrix inversion problem) involves a very large number of repetitive calculations, a task we send over to the digital computer (Bhaskaran & Collins, 2022).

2.1.2. Discretization using the finite-difference method

Consider the following one dimensional equation;

$$\frac{du}{dx} + u^m = 0; \;\; 0 \le x \le 1; \quad u(0) = 1$$

Let's start by considering the case where $m = 1$ when the equation is linear. We'll later consider $m = 2$ that is the case when the equation is nonlinear.

Derive a discrete representation of the above equation with $m = 1$ on the following grid:

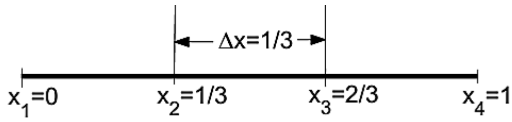

This grid has four equally-spaced grid points with Δx being the spacing between successive points. Since the governing equation is valid at any grid point, we have;

$$\left(\frac{du}{dx}\right)_i + u_i = 0$$

where the subscript i represents the value at grid point x_i. In order to get an expression for $(du/dx)_i$ in terms of u at the grid points, we expand u_{i-1} in a Taylor's series:

$$u_{i-1} = u_i - \Delta x \left(\frac{du}{dx}\right)_i + o(\Delta x)^2$$

Rearranging gives

$$\left(\frac{du}{dx}\right)_i = \frac{u_i - u_{i-1}}{\Delta x} + o(\Delta x)$$

The error in $(du/dx)_i$ due to the neglected terms in the Taylor's series is called the truncation error. Since the truncation error above is $o(\Delta x)$, this discrete representation is termed first order accurate.

Simplifying and excluding higher-order terms in the Taylor's series, we get the following discrete equation:

$$\frac{u_i - u_{i-1}}{\Delta x} + u_i = 0$$

This method of deriving the discrete equation using Taylor's series expansions is called the finite-difference method. However, most commercial CFD codes use the finite-volume or finite-element methods which are better suited for modelling flow past complex geometries.

2.1.3. Discretization using the finite-volume method

Consider an airfoil grid;

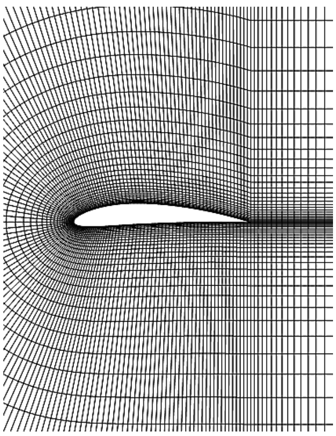

Figure 1: Airfoil grid

If you look closely at the airfoil grid shown earlier, you'll see that it consists of quadrilaterals. In the finite-volume method, such a quadrilateral is commonly referred to as a "cell" and a grid point as a "node". In 2D, one could also have triangular cells. In 3D, cells are usually hexahedrals, tetrahedrals, or prisms. In the finite-volume approach, the integral form of the conservation equations are applied to the control volume defined by a cell to get the discrete equations for the cell (Ramezani, et al., 2016). The integral form of the continuity equation for steady, incompressible flow is;

$$\int_{s} \vec{V}.\hat{n}ds = 0$$

The integration is over the surface S of the control volume and $\hat{n}$ is the outward normal at the surface. Physically, this equation means that the net volume flow into the control volume is zero.
Consider the rectangular cell shown below.

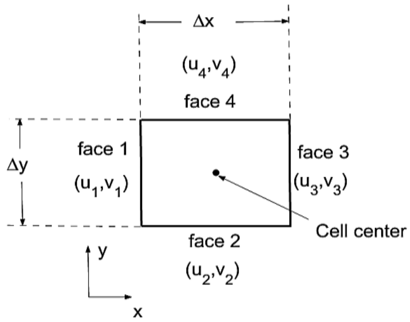

The velocity at face i is taken to be $\vec{V_i} = u_i\hat{\imath} + v_i\hat{\jmath}$. Applying the mass conservation equation above to the control volume defined by the cell gives;

$$-u_1\Delta y - v_2\Delta x + u_3\Delta y + v_4\Delta x = 0$$

This is the discrete form of the continuity equation for the cell. It is equivalent to summing up the net mass flow into the control volume and setting it to zero. So it ensures that the net mass flow into the cell is zero i.e. that mass is conserved for the cell. Usually, though not always, the values at the cell centres are solved for directly by inverting the discrete system.

The face values u_1, v_2, etc. are obtained by suitably interpolating the cell-centre values at adjacent cells. Similarly, one can obtain discrete equations for the conservation of momentum and energy for the cell. One can readily extend these ideas to any general cell shape in 2D or 3D and any conservation equation. Take a few minutes to contrast the discretization in the finite-volume approach to that in the finite-difference method discussed earlier.

Look back at the airfoil grid. When you are using a software like ANSYS, it's useful to remind yourself that the code is finding a solution such that mass, momentum, energy and other relevant quantities are being conserved for each cell. Also, the code directly solves for values of the flow variables at the cell centres; values at other locations are obtained by suitable interpolation (Versteeg & Malalasekera, 2007).

2.1.4. Assembly of discrete system and application of boundary conditions

Recall that the discrete equation that we obtained using the finite-difference method was

$$\frac{u_i - u_{i-1}}{\Delta x} + u_i = 0$$

Rearranging, we get

$$-u_{i-1} + (\Delta x + 1)u_i = 0$$

Applying this equation to the one dimensional grid shown earlier at grid points $i = 2, 3, 4$ gives;

$$-u_1 + (\Delta x + 1)u_2 = 0$$
$$-u_2 + (\Delta x + 1)u_3 = 0$$
$$-u_3 + (\Delta x + 1)u_4 = 0$$

The discrete equation cannot be applied at the left boundary $(i = 1)$ since u_{i-1} is not defined here. Instead, we can use the boundary condition to get;

$$u_1 = 1$$

Adding to the other equations above, we have the following simultaneous equations;

$$\begin{bmatrix} 1 & 0 & 0 & 0 \\ 1 & (\Delta x+1) & 0 & 0 \\ 0 & 1 & (\Delta x+1) & 0 \\ 0 & 0 & 1 & (\Delta x+1) \end{bmatrix} \begin{bmatrix} u_1 \\ u_2 \\ u_3 \\ u_4 \end{bmatrix} = \begin{bmatrix} 1 \\ 0 \\ 0 \\ 0 \end{bmatrix}$$

Generally, one would apply the discrete equations to the grid points (or cells in the finite-volume method) in the interior of the domain. For grid points (or cells) at or near the boundary, one would apply a combination of the discrete equations and boundary conditions. In the end, one would obtain a system of simultaneous algebraic equations with the number of equations being equal to the number of independent discrete variables. The process is essentially the same as for the model equation above with the details being much more complex.

ANSYS FLUENT, like other commercial CFD codes, offers a variety of boundary condition options such as velocity inlet, pressure inlet, pressure outlet, etc. It is very important that you specify the proper boundary conditions in order to have a well-defined problem. A single wrong boundary condition can give you a totally wrong result.

2.2. Finite Element Method

All continuous objects have infinite degrees of freedom, which make them unsolvable. FEM transforms these degrees of freedom to finite degrees of freedom with the help of discretization or meshing (creation of nodes and elements). The elements represent a finite number of pieces to which this numerical – computational method divides body. The nodes are where these pieces connect with each other (ANSYS, 2021). In general, FEM has the following advantages;

- It permits the creation of models of bodies with very complex shapes
- It can handle most loading/boundary conditions
- Here, it is possible to create accurate models of bodies made out of composite and multiphase materials.
- There can be variations in the element size and types.
- Analyses using this method can include time dependent and dynamic effects.
- It can handle a variety of nonlinear effects like material behaviour, large deformations, and boundary conditions just to name a few.

One can summarize the finite element method to the following steps;

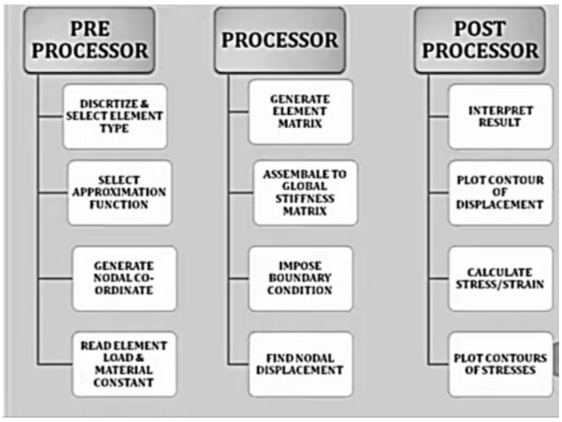

Figure 2: Steps of the finite element method

2.2.1. Types of elements in FEM

FEM/FEA solves problems by dividing the problem domain into a finite number of parts/cells/elements to which governing physics equations are applied. The final solutions are a combination of the results of the different element problem domains. These solutions could be deflections, stress, or strain at desired location or points in the object domain. Below are diagrams that differentiate the types of elements.

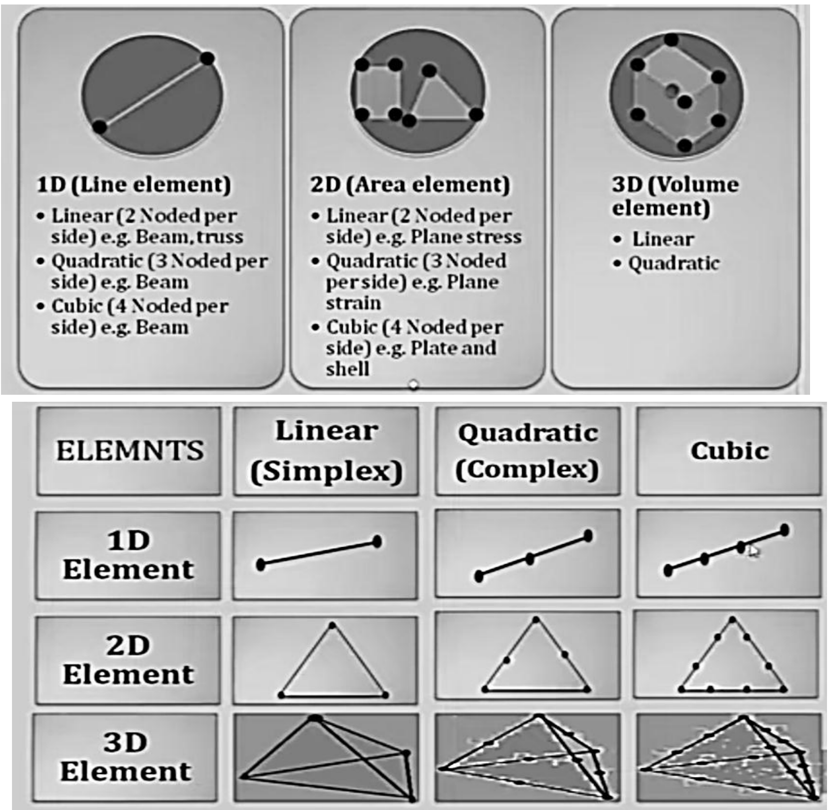

Figure 3: Different FEA Element Types

One can systematically select between the various FEA elements types using the steps that follow.

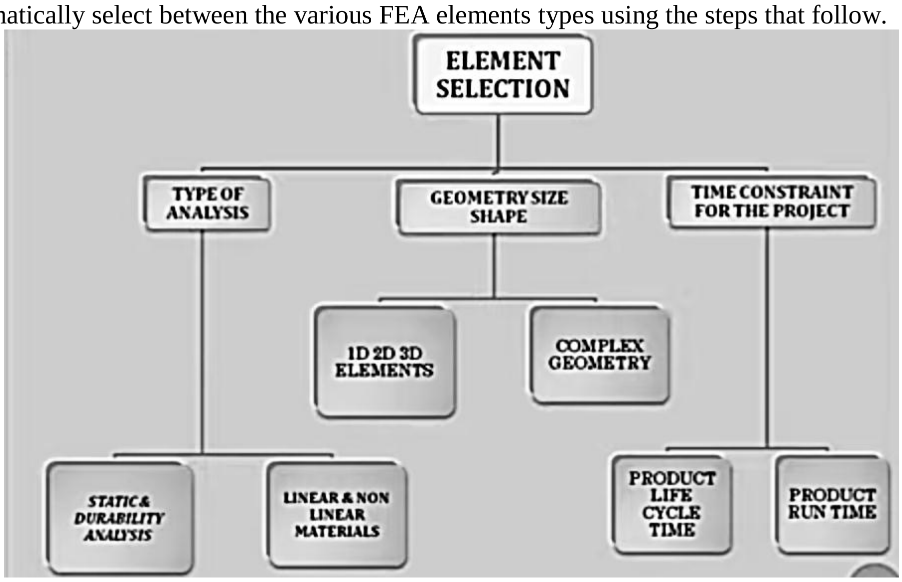

Figure 4: Elements selection

2.2.2. Types of FE analyses on ANSYS

ANSYS is software that realizes numerical analyses using the FEM. Some common FEA that one can run on any version of ANSYS include:

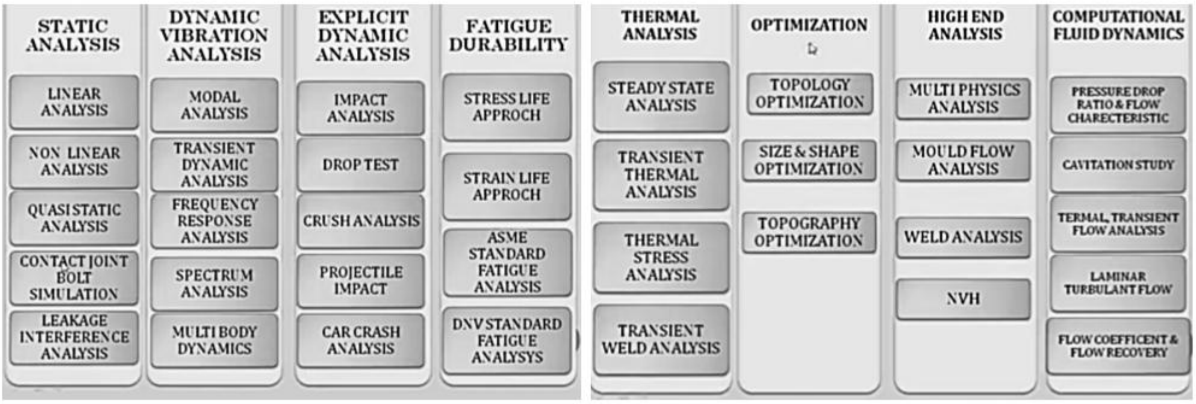

Figure 5: ANSYS FEA types

2.2.3. Modal analysis on ANSYS

The modal analysis identifies the natural frequency of a component part in an attempt to avoid resonance. ANSYS equally permits us to do the frequency response analysis that is the kind of testing that gives the point of excitation in the system (ANSYS, 2020). This test determines the resonance and the after effect on the system. Note that resonance is the phenomenon when the frequency of an external excitation matches the natural frequency of the system and the object vibrates at its maximum amplitude at this instant.

Modal analysis is a linear dynamics analysis. For solving the dynamic response of a structure, our basis is always the general equation of motion, where the unknows are acceleration, velocity and displacement for all points over the structure.

Equation of motion:

$$\boxed{\underbrace{[\boldsymbol{M}]}_{\text{Mass}}\underbrace{\{\ddot{\boldsymbol{u}}\}}_{\text{Acceleration}}+\underbrace{[\boldsymbol{C}]}_{\text{Damping}}\underbrace{\{\dot{\boldsymbol{u}}\}}_{\text{Velocity}}+\underbrace{[\boldsymbol{K}]}_{\text{Stiffness}}\underbrace{\{\boldsymbol{u}\}}_{\text{Displacement}}=\underbrace{\{\boldsymbol{f}(t)\}}_{\text{Load}}}$$

The modal analysis equation is an equation for a free and undamped system:

$$\boxed{[\boldsymbol{M}]\{\ddot{\boldsymbol{u}}\}+[\boldsymbol{K}]\{\boldsymbol{u}\}=\{0\}}$$

If we view this as a time domain dynamics problem, it basically describes a body sitting somewhere without motion or a body moving with a constant velocity. It's not meaningful to solve it and find the acceleration or displacement over time (ANSYS, 2020). Thus we have;

$$\boxed{\{\ddot{\boldsymbol{u}}(t)\}=0}$$

If we change our perspective and treat it as a frequency domain problem, we can find very interesting and meaningful results.

- How do we treat it as a frequency domain problem? Let's assume that every point of the structure is undergoing harmonic motion.
- What does a harmonic motion look like? Think of the oscillation of a simple spring-mass system. It's a periodic motion, which can be described by an amplitude, frequency and phase angle.

$$\boxed{x=\underbrace{A}_{\text{Amplitude}}\sin(\overbrace{\omega}^{\text{Angular Frequency}} t+\underbrace{\theta}_{\text{Phase angle}})}$$

Thus assume:

$$\{u\}=\{\phi\}_i\sin(\omega_i t+\theta_i)$$
$$\{\ddot{u}\}=-\omega_i^2\{\phi\}_i\sin(\omega_i t+\theta_i)$$

Substituting $\{u\}$and $\{\ddot{u}\}$ in the governing equation gives an eigenvalue equation:

$$([K]-\omega_i^2[M])\{\phi_i\}=0$$

From which we can calculate the natural circular frequencies ω_i and the mode shapes ϕ_i
Thus assumptions for modal analysis (ANSYS, 2015):

- $[K]$ and $[M]$ are constant:
  - Linear elastic material behavior is assumed
  - Small deflection theory is used, and no nonlinearities included
  - $[C]$ is not present, so damping is not included
  - $\{F\}$ is not present, so no excitation of the structure is assumed
  - The structure can be constrained or unconstrained
- Mode shapes $\{\phi_i\}$ are relative values, not absolute

When it is solved on a single DOF system (ANSYS, 2020):

$$\det([K] - \omega_i^2[M]) = 0$$

$$\omega = \sqrt{\frac{k}{m}} \qquad f = \frac{\omega}{2\pi}\,(\mathrm{Hz})$$

,

2.2.4. Fatigue analysis on ANSYS

In ANSYS we identify low cycle fatigue and high cycle fatigue. Low cycle fatigue is a fatigue failure when the number of stress cycles is less than 1000 while high cycle fatigue is a fatigue failure when the number of stress cycles is more than 1000. As the number of stress cycles increases, the component stress carrying capacity deceases and ANSYS quantifies this using the following rubrics (Browell, 2006).

- **Fatigue life**: number of cycles of fluctuating stress and strain of a specified nature that a material will sustain before failure occurs. The measure is time based, that is, in cycles, days, years, etc.
- **Fatigue damage**: it is the **ratio of design life over available life**. If this value is greater than **1**, the component will fail before the design life is attained.
- **Fatigue safety factor**: it shows the factor of safety with respect to the fatigue failure. It ranges from **1 to 15**. If the fatigue safety factor is less than 1 then the component will fail before the design life reaches.
- **Fatigue sensitivity**: it shows variations in the fatigue life, fatigue damage and fatigue safety factor when the current loading is varied (reduced or increased).

2.3. Material

To be able to realize the above studies on the engine design, a 3D model of the kinematics and dynamically acceptable design with $r_3 = 0.177$m and the volumes of its conduits were imported into ANSYS R18.2/2021 R2. Below are figures of the 3D model and the volumes of the various conduits.

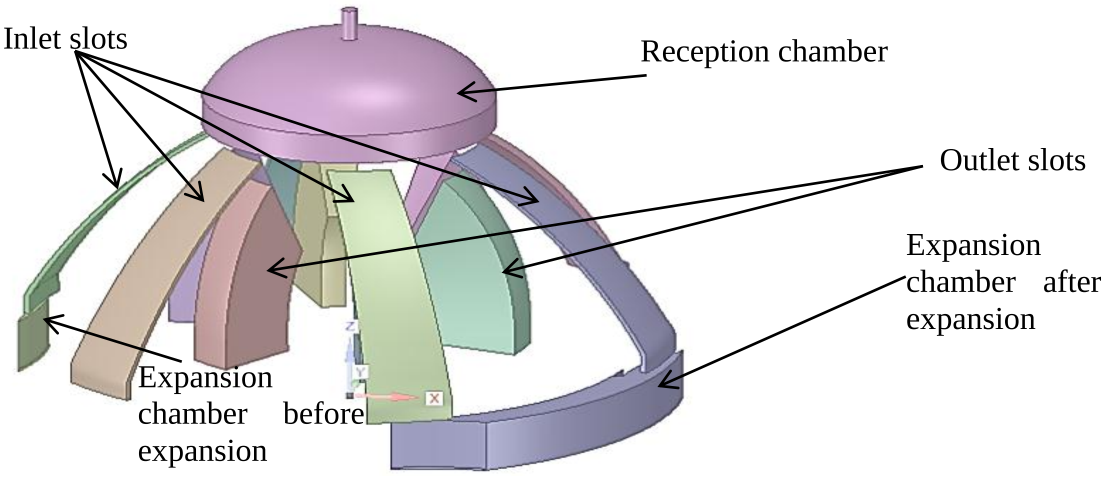

`

Figure 6: Principal volumes of compressed air engine

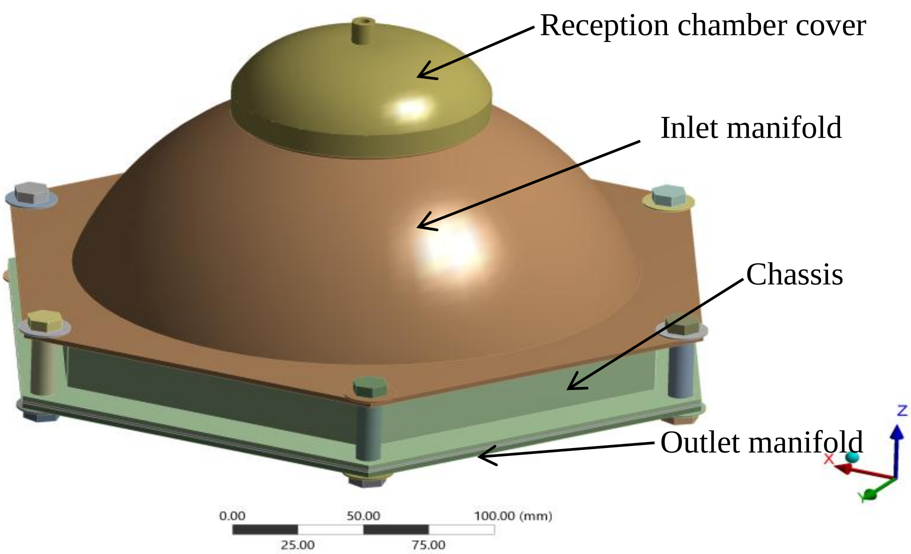

Figure 7: 3D picture of engine

III. Results and Interpretation

3.1. Computational Fluid Dynamics Simulations

We carried out this simulation to check flow of compressed air throughout the different conduits in an attempt to guarantee the presence of compressed air at their various destinations. We studied principally two sets of inlet – outlet pressures here; one to depict a scenario with the highest possible supply pressure and the second, one with lowest possible supply pressure. The paragraphs that follow represent our findings so far.

3.1.1. Flow with maximum supply pressure

Considering a supply pressure of 30MPa, after several simulations and redesigns of the conduits, we saw that compressed air would glide through the conduits into the expansion chamber. We find this in the velocity contour below, as there is some displacement of the compressed air all through to the lower end of the expansion chamber.

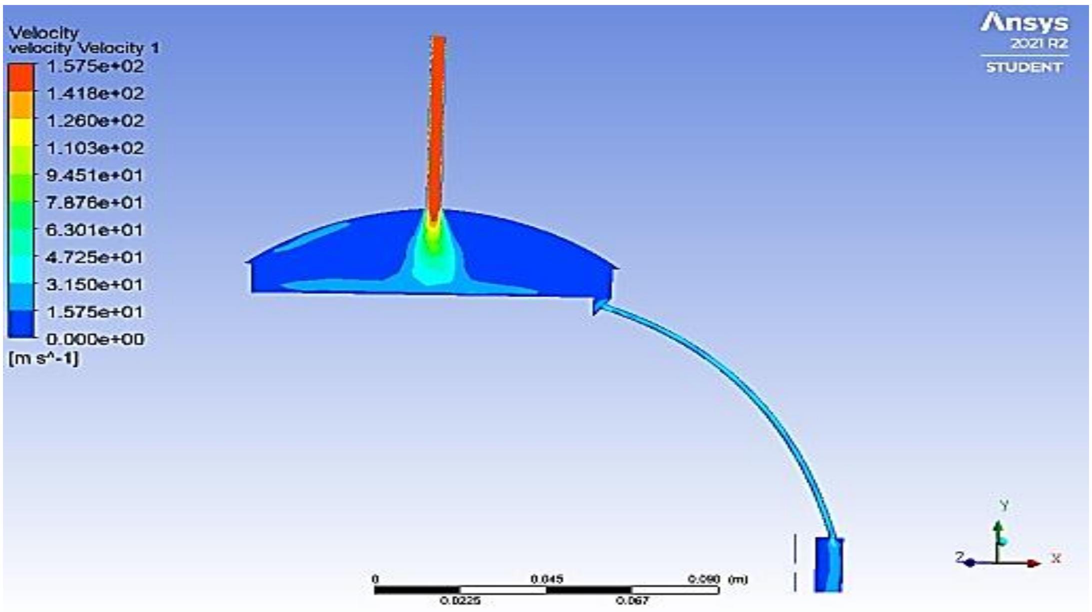

Figure 8: Velocity contour of input flow at maximum supply pressure

The pressure contour displayed an almost even distribution of the fluid's pressure across the stipulated pressure gradients from the intake to the outlet of the small conduits of the inlet manifold. This stipulates that the conduits are properly designed to handle perfect laminar flow of the compressed air at relatively very high pressure situations. Another conclusion drawn from such results is the fact that energy losses are brought to a minimum thus an improved efficiency of the entire engine design.

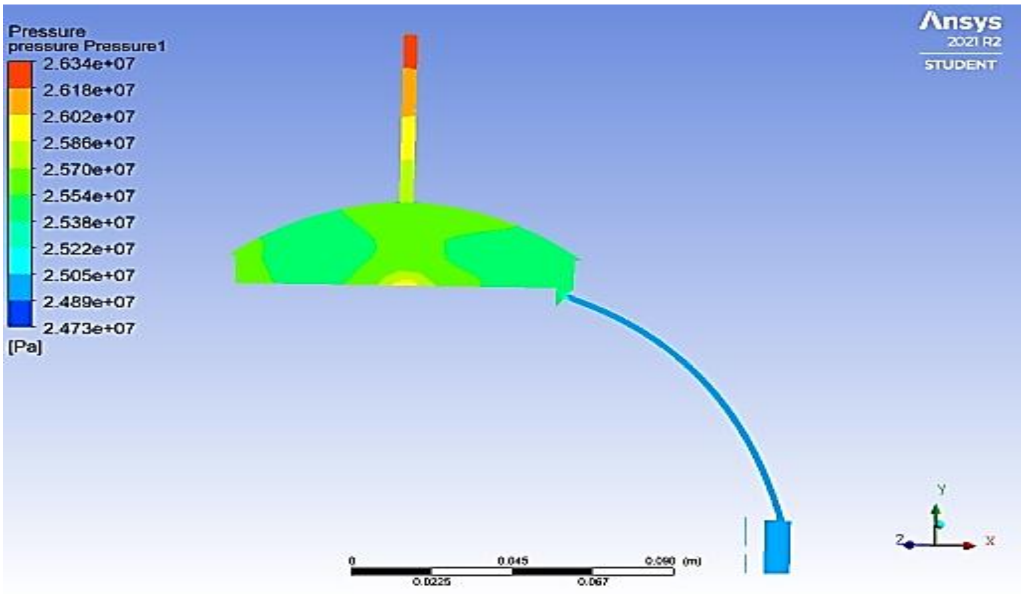

Figure 9: Pressure Contour of Input at Maximum supply pressure

3.1.2. Flow with minimum supply pressure

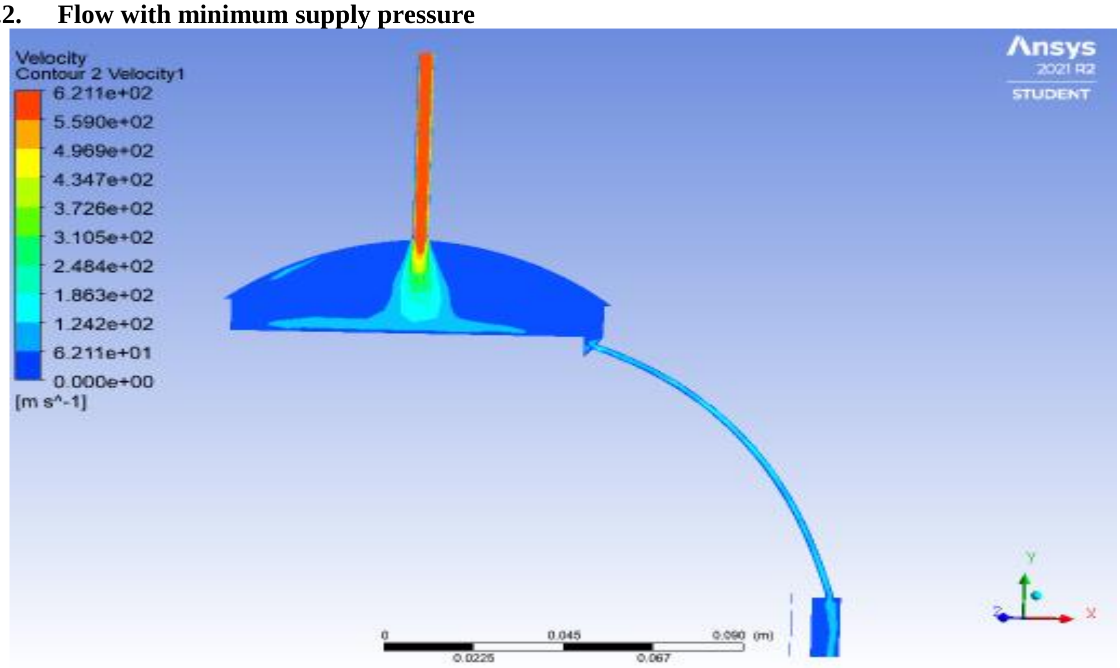

Figure 10: Velocity Contours of Input at minimum supply pressure

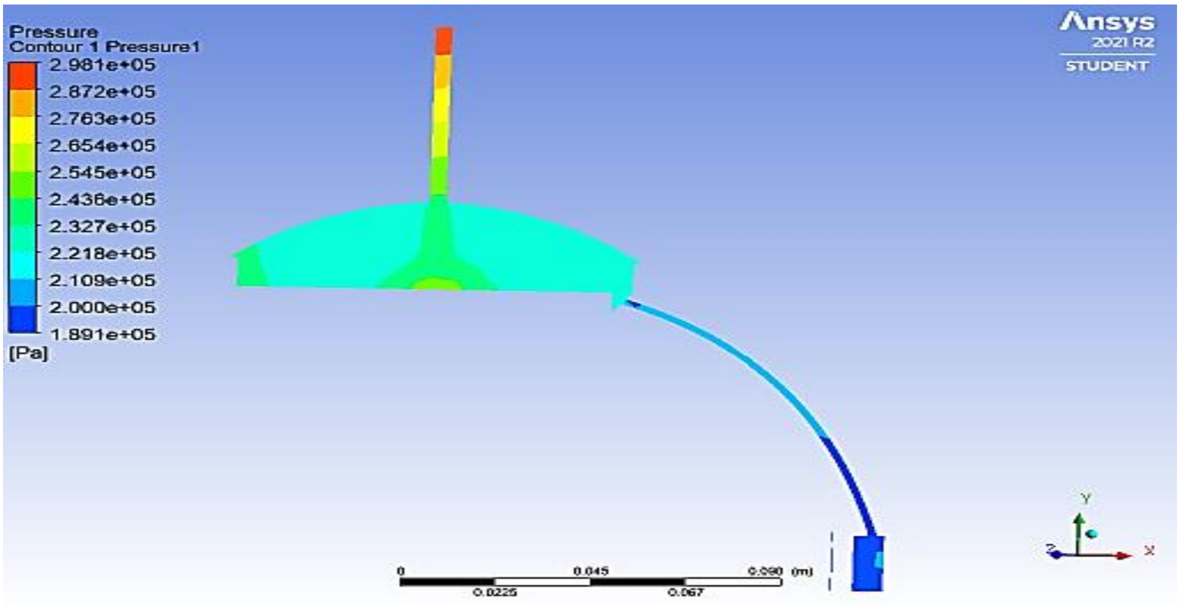

Figure 11: Pressure Contours of Input at minimum supply pressure

We considered a supply pressure of 5bars for this analysis. Though this is over 60 times less than the maximum, it was to guarantee the dexterity to pressure variations of the inlet manifold conduit assembly. We can identify some flow from the inlet down to the expansion chamber in the velocity contour and an almost linear distribution of the pressure over the selected pressure gradient. This implies the engine remains operational with compressed air of static pressure as low as 5bars.

3.2. Modal Analyses

Considering the rotor and the wings are the most susceptible parts of the engine to excessive vibrations, their modal analyses will help us understand their natural frequencies with mode shapes and their forced vibrational behaviors during certain frequency ranges.

3.2.1. Wings modal analyses

A wing model designed to fit the $r_3 = 0.177\text{m}$ dimension and subjected to further modal simulations gave the following results.
The natural frequencies were;

Table 1: Natural frequencies of the wings

Mode	Frequency [Hz]
1.	681.21
2.	2117.9
3.	3478.
4.	3810.6
5.	8685.2
6.	9727.4

The maximum speed of the engine is set at 6000rev/min thus 100rev/s, which implies we do not expect any external vibrations greater than 100Hz thus this wing design will not be subdued to any form of resonance throughout its useful life.
Further analysis for the harmonic response on application of a steady pressure of 30MPa revealed the following curve of the frequency response:

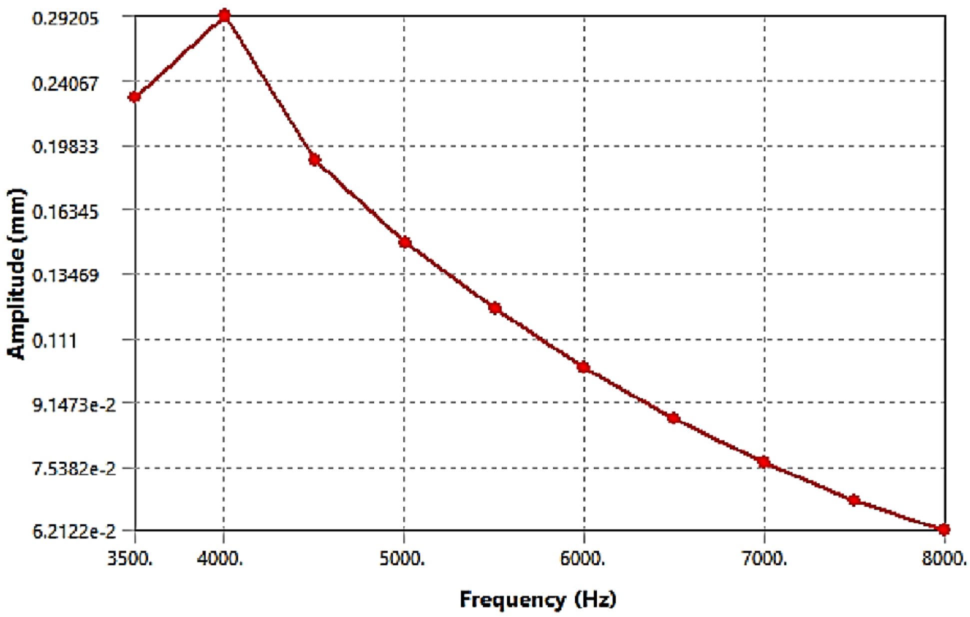

Figure 12: Frequency response curve of the wings

This indicates that if we force the wings to vibrate at 4000Hz, the expected maximum amplitude is 0.29205mm much lower than the 26.334mm total deformation the wing gets when subjected to a static pressure of 30MPa. The conclusion for this analysis is that the wings will withstand all the vibrations subjected to it by the engine.

3.2.2. Rotor shaft modal analyses

A rotor shaft model designed to fit the $r_3 = 0.177\text{m}$ dimension and subjected to further modal simulations gave the following results.
The natural frequencies were;

Table 2: Rotor shaft natural frequency

Mode	Frequency [Hz]
1.	282.71
2.	561.71
3.	766.14
4.	1573.1
5.	1761.4
6.	1829.4

The maximum speed of the engine is set at 6000rev/min thus 100rev/s, which implies we do not expect any external vibrations greater than 100Hz thus this rotor design will not be subdued to any form of resonance throughout its useful life.
Further analysis for the harmonic response on application of a steady pressure of 30MPa revealed the following curve of the frequency response:

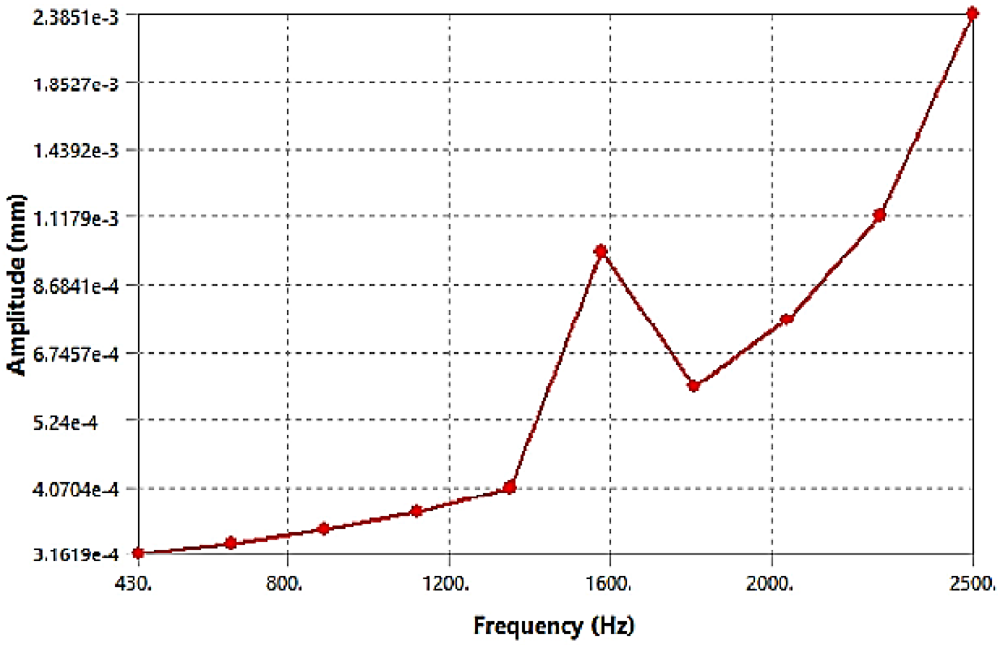

Figure 13: Frequency response curve of the rotor shaft

This indicates that if we force the rotor shaft to vibrate at 1600Hz, the expected maximum amplitude is 0.29205mm much lower than the 26.334mm total deformation the wing gets when subjected to a static pressure of 30MPa. The conclusion for this analysis is that the wings will withstand all the vibrations subjected to it by the engine.

3.3. Fatigue Analyses

From previous static analyses of the compressed air engine design, the assembly technic had a major role to play on the stress resistance of the engine. When realizing the fatigue analyses, they took into consideration this effect thus instead of realizing a fatigue analyses of the different components surrounding the high stress zone of the engine, the analyses involved an assembly of the components in the high stress zone.

This study involved various simulations with modifications of the dimensions of the components so that they have a longer useful life. The results below represent that of the most acceptable engine design. The modifications included material changes, as structural steel happened to be the only material with all alternation stress parameters in the ANSYS version used to do the simulations.

Because of the modifications done on the engine, they did again a second static structural simulation of the assembly. Studies realized included the total deformation analyses and safety factor of the fatigue analyses. The concluding results are as follows:

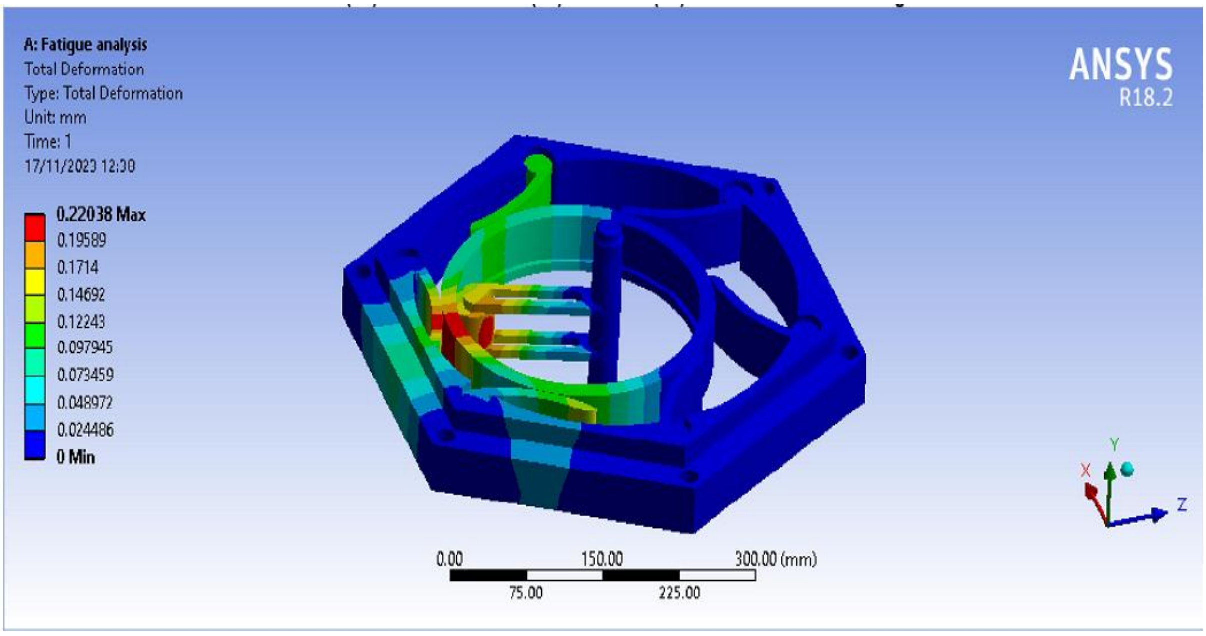

Figure 14: Total Deformation analyses

The new engine design improves significantly the maximum total deformation of the engine. The maximum deformation saw a shift from 5.6343mm in the previous design to 0.2208mm in the new design even though the external loads and boundary conditions remain the same.

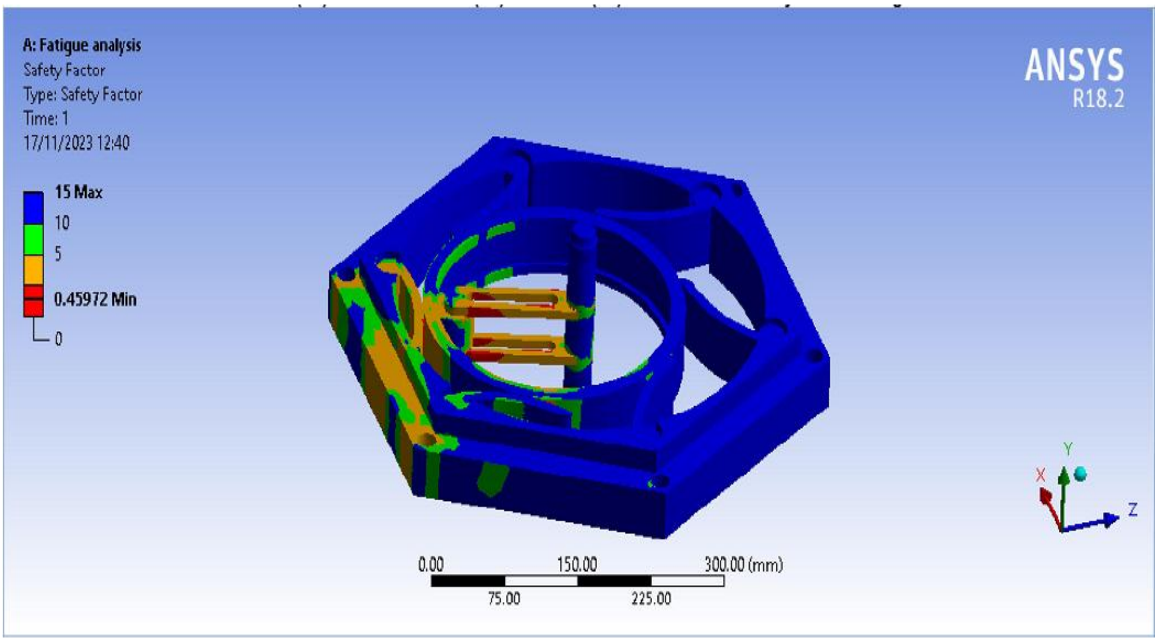

Figure 15: Fatigue Safety factor for static loading

The safety factor analysis for a static load of 30MPa in the expansion chamber was even more impressive as only an almost negligible portion of the rotor seems to show signs of failure before its design period.

Further fatigue analysis of the design included a zero – base alternating load analysis. They used the same boundary conditions for this exercise as above but for the pressure in the combustion chamber that vary from 30MPa to 0 per cycle repeatedly. The simulation was a strain fatigue simulation implying the exercise considered the life of the parts until the appearance of a crack. The execution of the exercise was in accordance

to with the Mean Stress Correction Theory. The results include; the fatigue life analysis, fatigue damage analysis, fatigue safety factor analysis and the fatigue sensitivity curve.
The results on the life analysis included a repeated simulation of alternating loads from 0 to 30MPa until the appearance of cracks on the parts. Note that, 10^6 cycles are the number of operation cycles for a part to survive its design life.

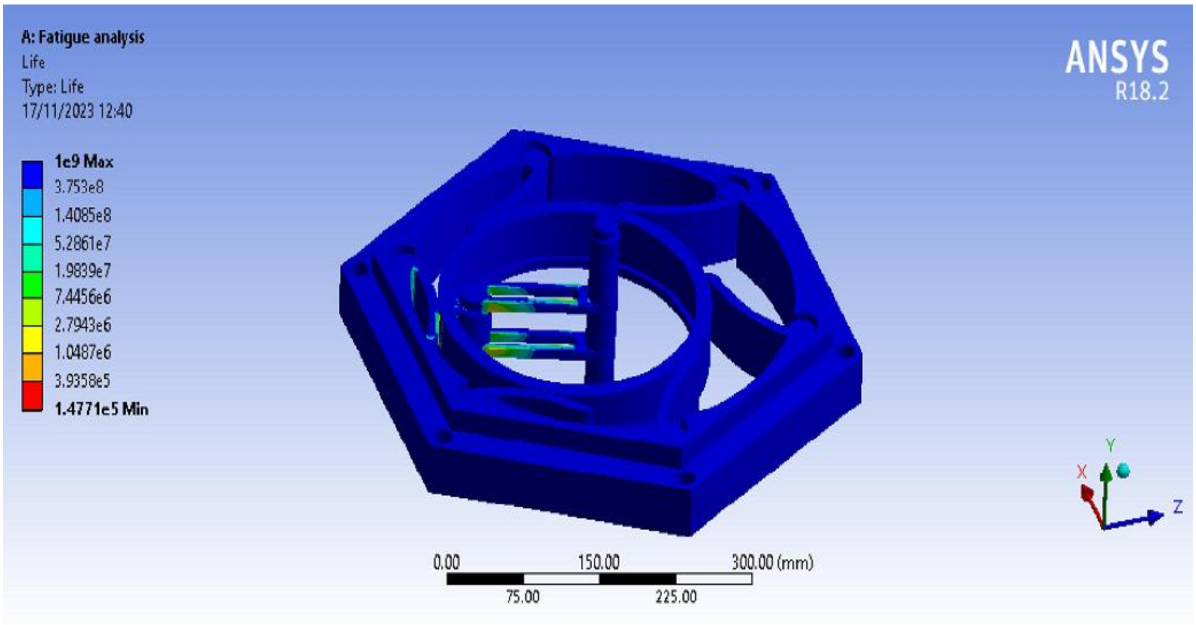

Figure 16: Fatigue life analysis with alternating load solicitations

From the above plots, almost all the parts have their life exceed their design life. The useful lives below the design life are almost inexistent. This is a clear indication of the resistance of the parts to fatigue and thus the longevity of the engine under operation.

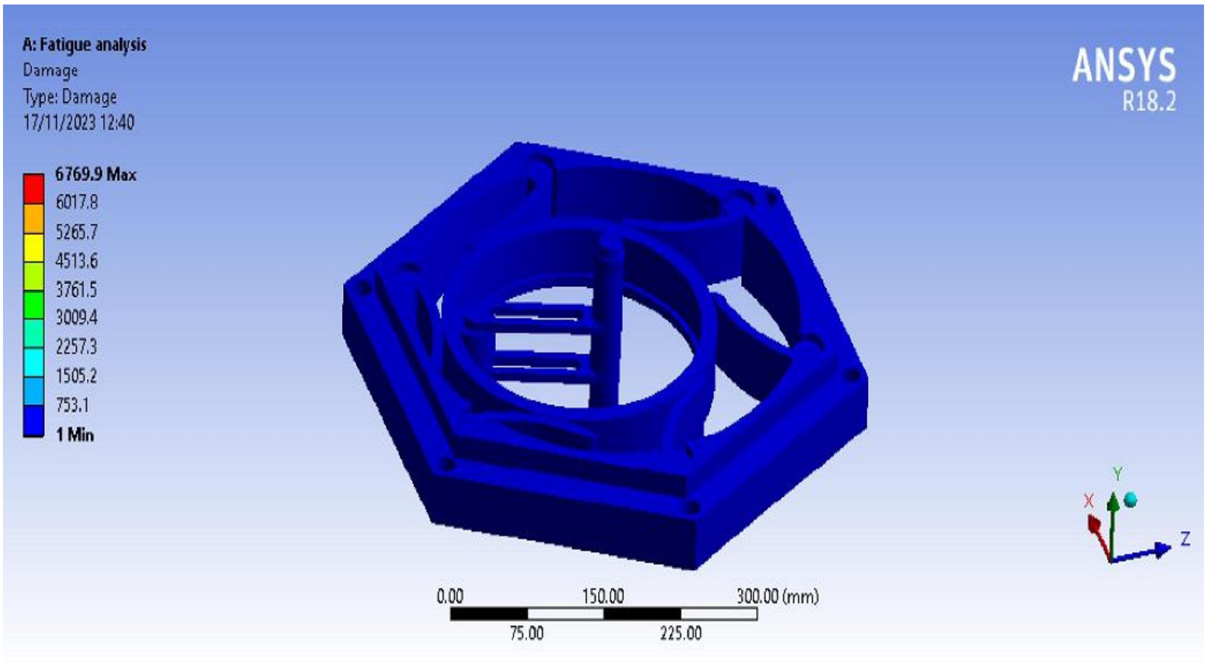

Figure 17: Fatigue damage analysis with alternating load solicitations

The fatigue damage analysis draws conclusion on the relation between the available life and the design life of each part. The plot being completely blue implies all the designed parts have available lives equal to their design lives. Thus, they are not prone to fatigue in the life span of the engine.

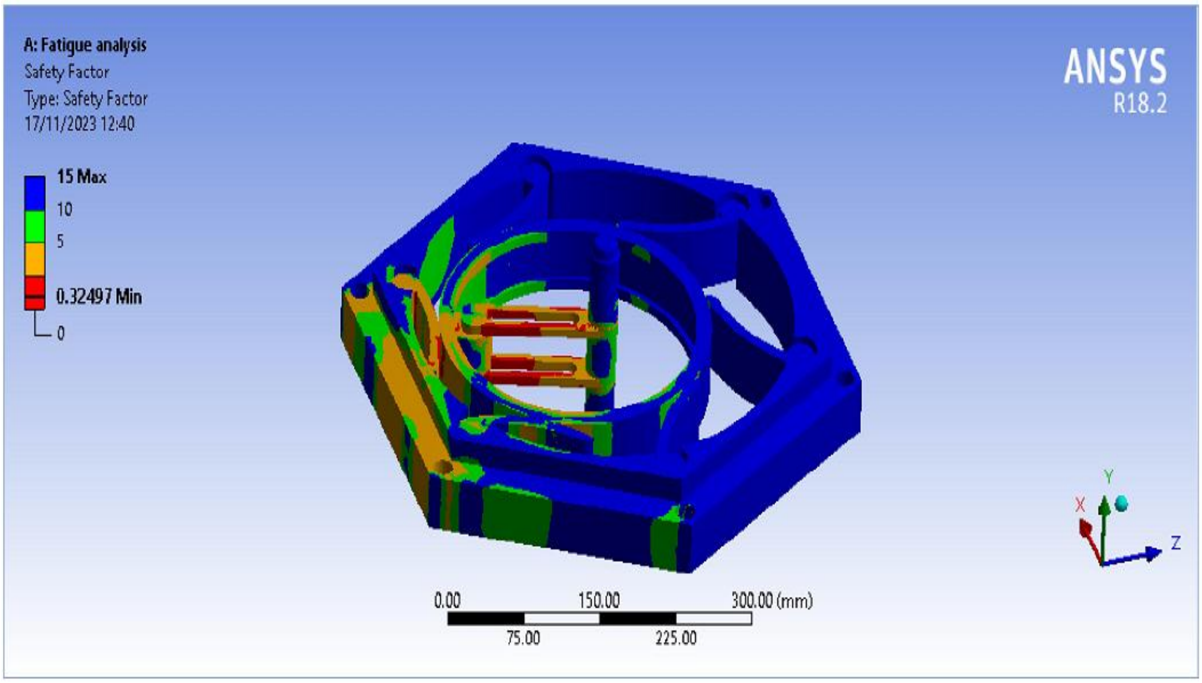

Figure 18: Fatigue safety factor analysis with alternating load solicitations

The safety factor goes further to identify just a hand fold of part areas susceptible to have cracks but these are just a minute portion of the parts that is, negligible. This is an assuring fact that the engine is designed to last long under such solicitations.

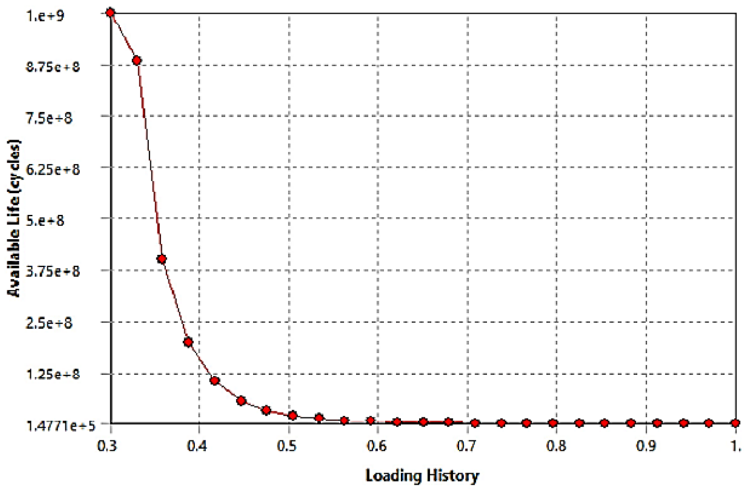

Figure 19: Fatigue Sensitivity Analysis with alternating load solicitations

Considering the 30MPa pressure is the maximum pressure of the intake compressed air to the engine, this analysis considered the possible life cycles of scenarios where the pressure is lower than the 30MPa which will obviously be the case, considering the engine is designed to obtain its maximum power at pressures as low as 10MPa. The results of the studies brought out the conclusion that if the peak pressure value was set at 10MPa or less, the engine will operate in indefinitely with none of its components failing nor having a fault as small as a crack.

An engine with such remarkable performance theoretically, is set for prototype production. Findings from the modal and fatigue analyses helped fortify the readiness of the design, not just at the level of its functionality but also at the level of its resistance to accrued stress values. Thus, the engine design is capable of realizing its functional expectations as well as its structural expectations.

3.4. Engine Design Presentation

This chapter consists of the presentation of the validated engine design. This is a step closer to the establishment of a patented model of the engine design. There are detail dimensions of some elements and subassemblies of the engine and the final material allocation of the engine.

Name of part	Chassis	Rotor assembly
Calibrated Diagram	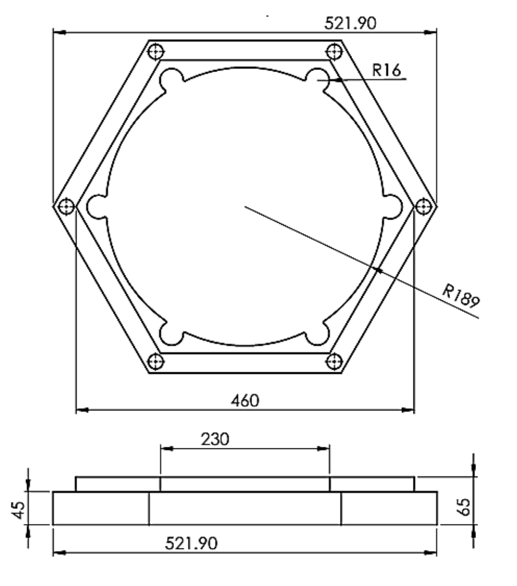	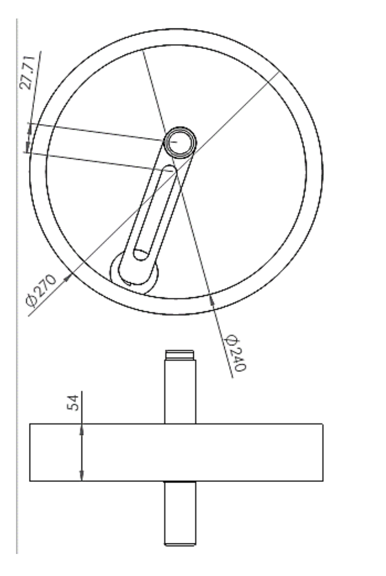

Figure 20: Calibrated diagrams of chassis and rotor assembly

Table 3: Final Materials allocations

ITEM NO.	PARTS	MATERIALS	QTY.
1	Chassis	AISI 4130 Steel, normalized at 87deg.C	1
2	Wings	AISI 4130 Steel, normalized at 87deg.C	6
3	Inlet Manifold	Gray Cast Iron	1
4	Rotor shaft	AISI 4130 Steel, normalized at 87deg. C	1
5	Rotor bearings	AISI 4130 Steel, normalized at 87deg.C	1
6	Rotor cylinder	AISI 4130 Steel, normalized at 87deg.C	1
7	Outlet Manifold	Gray Cast Iron	1
8	Hexagon Nut ISO M10	AISI 4130 Steel, normalized at 87deg.C	6
9	Hexagon Bolts ISO M10	AISI 4130 Steel, normalized at 87deg.C	6
10	Timer	Gray Cast Iron	1
11	Reception Chamber Cover	AISI Type 316L stainless steel	1

IV. Conclusion

This article projects how we acquired acceptable material/external dimensions of a zero CO_2 and zero heat pollution compressed air engine for the urban transport sector from our understanding of its internal dimension through a series of CFD, modal and fatigue numerical simulations on ANSYS R18.2/2021 R2. The end result were complete acceptable dimensions of the various component parts of the engine and their final material allocations.

The end model of the engine from this studies is over dimensioned to withstand all the possible solicitations the engine is susceptible to face during its functioning. To this effect, ANSYS alongside SOLIDWORKs estimated the production cost of an engine prototype at 7 million FCFA with an initial weight of 132 963.73g and the engine occupying a volume of $0.02m^3$ for a surface space of $1.76m^2$. These information permits us to accurately picture the engine prototype which makes us even more prepared to create an up to scale prototype of the engine.

References

[1]. Albritton, D., 1998. What Should Be Done in a Science Assessment In Protecting the Ozone Layer: Lessons, Models, and Prospects, s.l.: ResearchGate.
[2]. Angell, J. K. & Korshover, J., 2005. Quasi-biennial and Long-term Fluctuations in Total Ozone. Monthly Weather Review vol. 101, p. 426–443.
[3]. ANSYS, 2015. Modal Analysis. 16 ed. Southpointe: ANSYS Inc.
[4]. ANSYS, 2020. Application of Modal Analysis. Southpointe: ANSYS Inc.
[5]. ANSYS, 2020. Governing Equations of Modal Analysis. Southpointe: ANSYS Inc.
[6]. ANSYS, 2020. Intro to Modal Analysis. s.l.:ANSYS.
[7]. ANSYS, 2021. Ansys Fluent Theory Guide. Southpointe: ANSYS Inc.
[8]. Bhaskaran, R. & Collins, L., 2022. Introduction to CFD Basics. Upson Hall: Sibley School of Mechanical and Aerospace Engineering.
[9]. Browell, R., 2006. Calculating and Displaying Fatigue Results. Al Hancq: ANSYS, Inc.
[10]. Childs, P., 2021. Mechanical Design: Theory and Applications. s.l.:Elsevier Science.
[11]. Craig, K., 2011. Fundamental Principles of Mechanical Designs. s.l., s.n.
[12]. Department of Climate Change Australia, 2008. National Greenhouse Gas Inventory (2006). s.l.:Australian Government.
[13]. Fergusson, A., 2001. Ozone layer Depletion and Climate Change: Understanding the linkage. Canada: Minister of Public Works and Government Services Canada.
[14]. Heinberg, R., 2011. Rising Cost of Fossil Fuels and the Coming Energy Crunch. OILPRICE.COM, 12 July.
[15]. International Energy Agency, 2009. Transport, Energy and CO2. Directorate of Sustainable Policy and Technology.
[16]. K., M. M., P.Rathod, D. & Arvind S., P. S., 2012. Study and Development of Compressed Air Engine Single Cylinder: A Review Study. International Journal of Advanced Engineering Technology, pp. 271-274.
[17]. K.T. Chau, 2014. 21 - Pure electric vehicles. In: Alternative Fuels and Advanced Vehicle Technologies for Improved Environmental Performance. s.l.:Woodhead Publishing, p. 655 – 684.
[18]. Kahn, B., 2016. World's Atmospheric Carbon Dioxide Passes 400 PPM Threshold. Permanently. Climate Central, 27 September.
[19]. Kavalec, C., 1999. Vehicle choice in an aging population: Some insights from a stated preference survey from California. The Energy Journal, pp. 20(3), 123-138.
[20]. Kronberg, N. & Shawn, W., 2019. Transport Statistics Great Britain. Department of Transport.
[21]. Lambert, J., 2020. Emissions Dropped during the COVID-19 pandemic.. Science News, 7 August.
[22]. Leer, B. v. & Powell, K. G., 2021. Introduction to Computational Fluid Dynamics. Michigan: University of Michigan.
[23]. Malay, J., Ritik, J., Harshvardhan, P. & Yash, P., 2021. Design & Working of Compressed Air Engine. International Research Journal of Engineering and Technology, pp. 2399-2401.
[24]. Morrisette, P. M., 1995. The Evolution of Policy Responses to Stratospheric Ozone Depletion. Natural Resources Journal, p. Vol 2.
[25]. Ngang Tangie Fru, 2019. Zero CO2 and Zero Heat Pollution Compressed Air Engine for the Urban Transport Sector, Yaounde Cameroon: University of Yaounde 1.
[26]. Ngang, T. F., 2019. Zero CO2 and Zero Heat Pollution Compressed Air Engine for the Urban Transport Sector, Yaounde Cameroon: University of Yaounde 1.
[27]. Odd André, H., Arnesen, P., Torstein, A. B. & Sondell, R. S., 2020. Estimation of tank-to-wheel efficiency functions based on type approval data. Applied Energy, p. Vol 276.
[28]. Plumb, J., 2023. A Deep Dive into Engineering Design Principles and Methodology. Cambridge Design Technology.
[29]. Ramezani, A., Stipcich, G. & Garcia, I., 2016. Introduction to Computational Fluid Dynamics. s.l.:Basque Center for Applied Mathematics.
[30]. Rucks, J. W. a. G., 2015. 5 steps to an urban transportation revolution. GreenBiz, 17 March.
[31]. Sivasakthivel, T. & K.K. Siva, K. R., 2011. Ozone Layer Depletion and Its Effects: A Review. International Journal of Environmental Science and Development.
[32]. Society, N. G., 2023. Ozone Layer. [Online]
[33]. Available at: https://education.nationalgeographic.org
[34]. Stoevesandt, B., Steinfeld, G. & Höning, L., 2017. Computational Fluid Dynamics. OLDENBURG: Carl von Ossietzky University of Oldenburg.
[35]. Thipse, S., 2008. Compressed air car. TECH MONITOR, Nov-Dec.
[36]. Thipse, S., 2008. Compressed Air Car. Engine Development Laboratory: s.n.
[37]. Thompson, A., 2016. August Declared Hottest on Record: NASA. Climate Central, 14 September.
[38]. Tian, H. et al., 2023. Advancements in compressed air engine technology and power system integration: A comprehensive review. Science Direct.

[39]. Verma, S., 2008. Air Powered Vehicle. The Open Fuels & Energy Science Journal, pp. 54-56.
[40]. Versteeg, H. K. & Malalasekera, W., 2007. An Introduction to Computational Fluid Dynamics Finite Volume Method. Edinburgh Gate: Pearson Education Limited.